Supplementary Information for

Ultrafast metal corrosion engineering facilitates the construction of CoS$_x$ derived from MOFs as enhanced supercapacitor electrodes

Hao Chen[a], Xuehua Yan[a,b,*], Jianmei Pan[a], Zohreh Shahnavaz[b], Jamile Mohammadi Moradian[b]

[a]*School of Materials Science and Engineering, Jiangsu University, Zhenjiang 212013, Jiangsu, P. R. China*

[b]*Institute for Advanced Materials, Jiangsu University, Zhenjiang 212013, Jiangsu, P. R. China*

*Corresponding author: Xuehua Yan; E-mail address: xhyan@ujs.edu.cn; Tel. & Fax: 86 511 88790798.

E-mail: xhyan@ujs.edu.cn

Materials characterizations

X-ray diffraction (XRD, Rigaku SmartLab SE) analysis was employed to determine the crystal structure (5-90°, Cu Kα, λ = 0.15418 nm). The chemical bonds and functional groups were investigated using Fourier-transform infrared spectroscopy (FTIR, Thermo Scientific Nicolet iS20). The FTIR test was conducted in ATR (Attenuated Total Reflection) mode, with a resolution of 4 cm^{-1} and 32 scan repetitions. The tested wavenumber range was from 400 cm^{-1} to 4000 cm^{-1}.The elemental composition and valences were explored using X-ray photoelectron spectroscopy (XPS, Thermo Scientific K-Alpha). XPS analysis was conducted using a monochromatic Al Kα source (hv=1486.6 eV, 6 mA, 12 kV). The C1s binding energy of 284.80 eV was used as the energy standard for charge correction. The analysis area was set at 400 μm spot size. Full-spectrum scans were conducted with a pass energy of 100 eV and a step size of 1 eV. Additionally, narrow-spectrum scans were performed at least 5 times with a pass energy of 50 eV and a step size of 0.1 eV for each cycle, to accumulate signals and enhance the resolution. Scanning electron microscopy (SEM, ZEISS GeminiSEM 300) with an energy-dispersive spectroscopy (EDS) detector was employed to examine the product morphology and element distribution. A high-resolution TEM (HRTEM, TF-20, 200kv) with energy dispersive X-ray spectroscopy (EDX), and a transmission electron microscopy (TEM, HT-7800, 120 kv) are used to characterize the morphology and composition of samples.

Electrochemical measurements

The electrochemical performance of the fabricated material was evaluated using a three-electrode system on an electrochemical workstation (ShangHai ChenHua, CHI 760E). The cyclic voltammetry (CV), galvanostatic charge-discharge (GCD), and

electrochemical impedance spectroscopy (EIS) tests were conducted. The prepared material, platinum electrode, and Ag/AgCl electrode were used as the working electrode, counter electrode, and reference electrode, respectively. Prior to testing, the electrode materials were immersed in a 3 M KOH solution for 0.5 hours to ensure sufficient penetration.

According to the GCD curve, the areal capacitance (C_s, F cm^{-2}) and specific capacitance (C_m, A g^{-1}) are calculated by the following equation [1, 2].

$$C_s = \frac{I \times \Delta t}{S \times \Delta V} \#(E1)$$

$$C_m = \frac{I \times \Delta t}{m \times \Delta V} \#(E2)$$

Where I(A), t(s), V(V), S(cm^2) and m(g) represent current density, discharge time, voltage window, area of the active substance and mass of the active substance, respectively.

Fabrication and electrochemical analysis of the Asymmetric supercapacitor (ASC).

A ASC was constructed using CoS_x@NiFe-S@NF composite material as the positive electrode and activated carbon (AC) as the negative electrode. The negative electrode was prepared by mixing 80 wt% AC, 10 wt% acetylene black, and 10 wt% polyvinylidene fluoride (PVDF) in N-methyl-2-pyrrolidone (NMP). The resulting slurry was uniformly coated onto a clean carbon cloth current collector and dried overnight under vacuum conditions at 60 °C. PVA/KOH gel electrolyte was used, and its electrochemical performance was investigated.

For a two-electrode system, the mass specific capacitance of $CoS_x@NiFe-S@NF$ is 1926 F g^{-1}. We calculate the mass loading of the positive and negative electrodes according to the mass balance equation [3]:

$$\frac{m_+}{m_-} = \frac{C_{m-} \times \Delta V_-}{C_{m+} \times \Delta V_+} \#(E3)$$

where m (g), C_m (F g^{-1}), ΔV (V) are the mass load, specific capacitance, and operating voltage window of the positive (+) and negative (-) electrodes, respectively.

The specific capacity (C_m, F g^{-1}), energy density (E) and power density (P) of an asymmetric supercapacitor (ASC) can be calculated by the following formula[2]:

$$C_m = \frac{I \times \Delta t}{m \times \Delta V} \#(E4)$$

$$E = \frac{C \times \Delta V^2}{2 \times 3.6} \#(E5)$$

$$P = \frac{3600E}{\Delta t} \#(E6)$$

Where I, Δt, ΔV, m(g), respectively represent the current density, discharge time, and the voltage window of the ASC and the total weight of the active substance loaded on the two electrodes.

The potential formation mechanism of the hollow structure are as follows:

S^{2-} reacts with the Co^{2+} on the surface of ZIF-L, producing a layer of cobalt sulfide buffering layer. Subsequently, for further sulfidation of ZIF-L, both Co^{2+} and S^{2-} need to pass through this buffering layer. Given the smaller ionic radius of Co^{2+} (Co^{2+} = 70 pm, S^{2-} = 184 pm), Co^{2+} is more likely to diffuse outward through the buffering layer than S^{2-}, which is difficult to diffuse inward. Consequently, Co^{2+}

within ZIF-L gradually diffuses to the exterior of the cobalt sulfide buffering layer. Concurrently, it reacts with S^{2-} to generate sulfide, and internally, the metal-organic framework dissolves due to Co diffusion. This process leads to the formation of the observed hollow structure [4, 5].
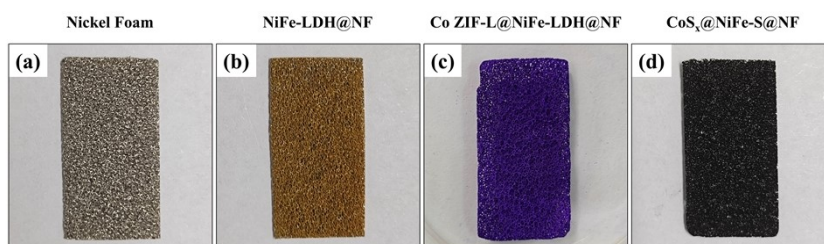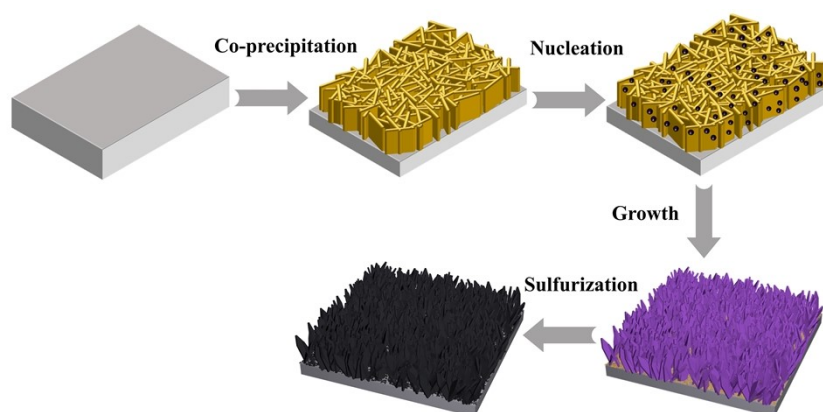

Fig. S1 Real image of electrodes.

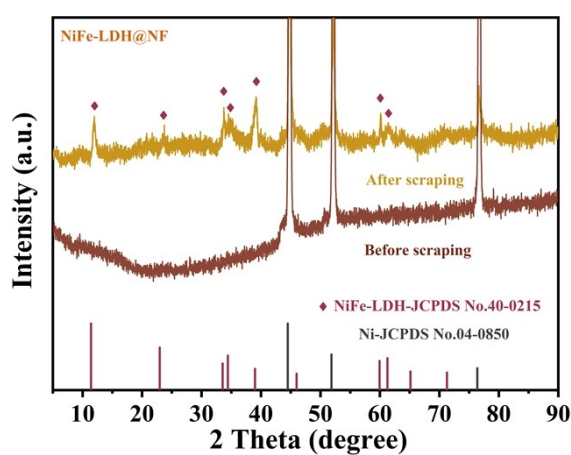Fig. S2 Schematic diagram of nucleation and growth of Co ZIF-L.

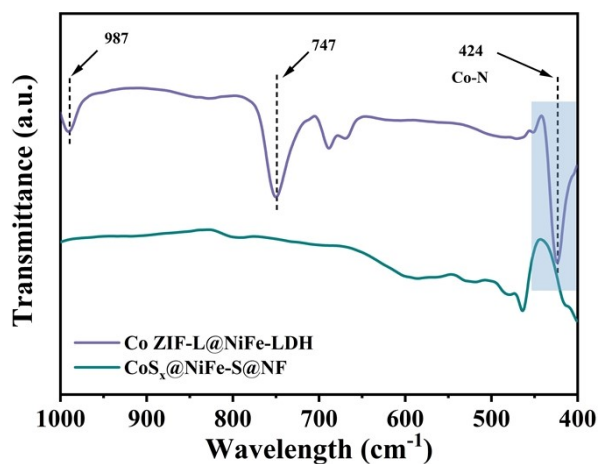Fig. S3 XRD patterns of NiFe-LDH@NF.

Fig. S4 FTIR spectra of Co ZIF-L@NiFe-LDH@NF and CoS$_x$@NiFe-S@NF in the range of
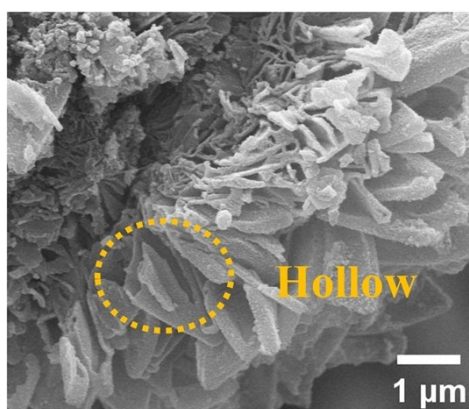
400-1000 cm^{-1}.

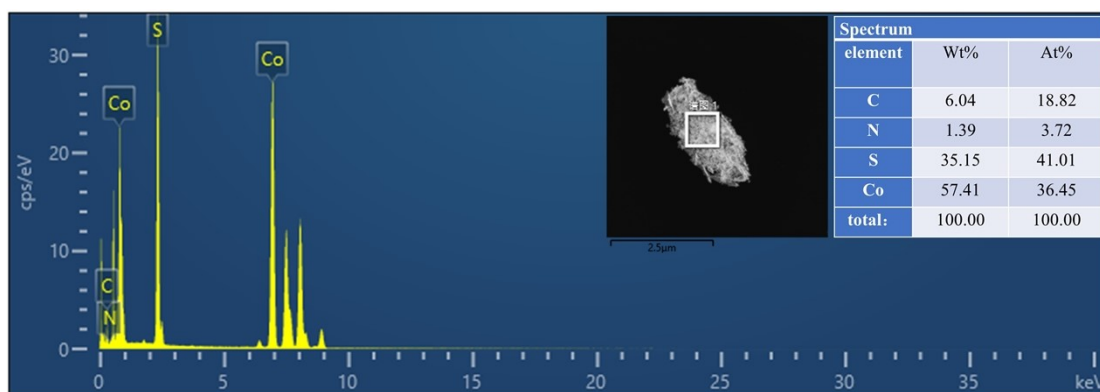Fig. S5 SEM of image of Hollow Structure CoS$_x$.

Spectrum		
element	Wt%	At%
C	6.04	18.82
N	1.39	3.72
S	35.15	41.01
Co	57.41	36.45
total：	100.00	100.00

Fig. S6 The semi-quantitative EDX elemental analysis results for the selected region of CoS$_x$.
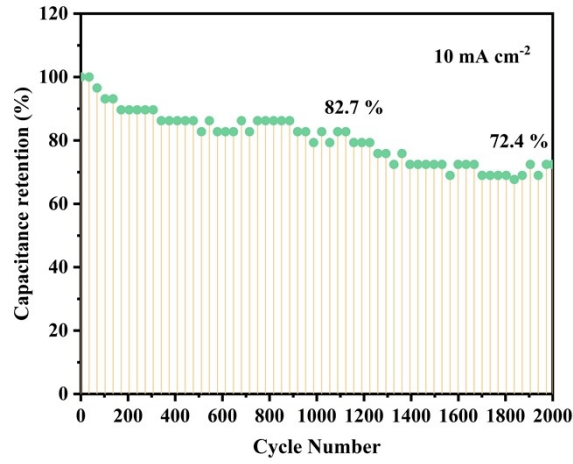
Fig. S7 (a) cyclic stability of $CoS_x@NiFe-S@NF$ at 10 mA cm^{-2}.
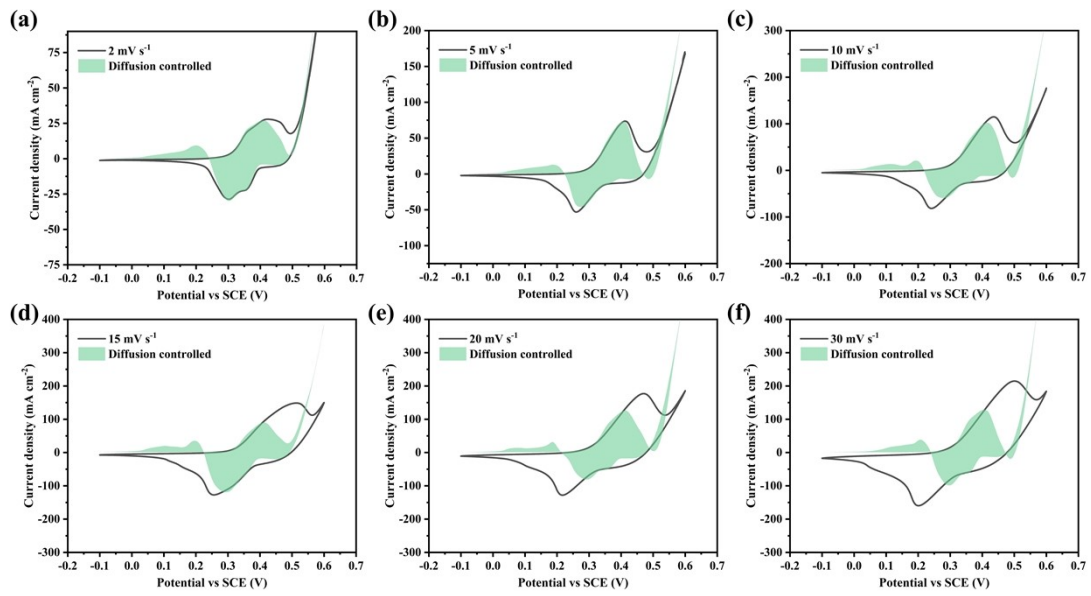

Fig. S8 Graphs of raw CV vs surface-controlled CV at 2-30 mV s^{-1}.
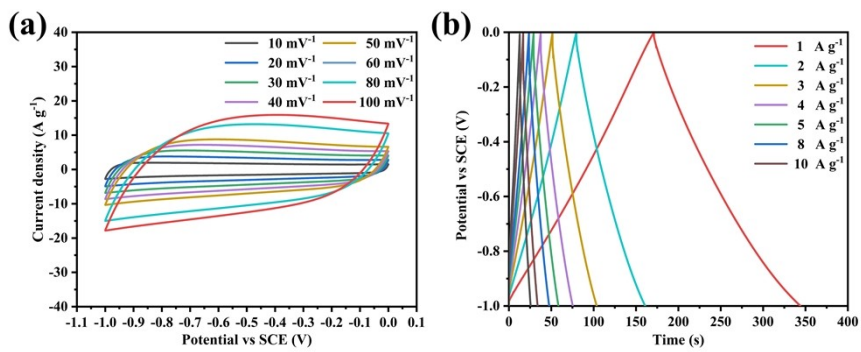

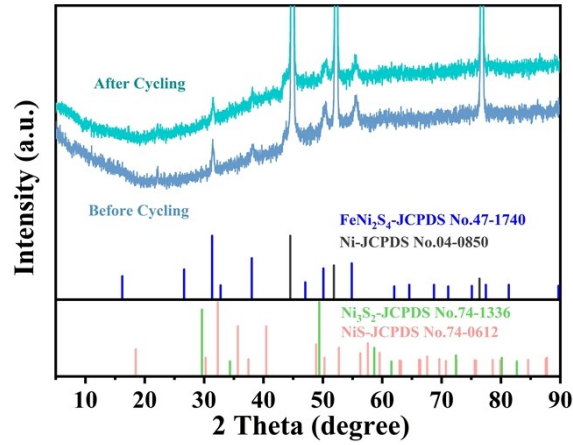Fig. S9 (a) CV curves of AC electrode, (b) GCD curves of AC electrode.

Fig. S10 XRD pattern of CoS$_x$@NiFe-S@NF before and after cycling tests.

Table S1 XPS semi-quantitative analysis results for Co^{2+} and Co^{3+}.

Element	Peak position	FWHM eV	Area(p) CPS.eV	Atomic %
Co^{2+}	779. 6	3. 19	14687. 83	21. 21
Co^{3+}	781. 5	3. 02	54447. 12	78. 79

Table S2. The numerical values of each component in the equivalent circuit of the impedance spectrum in Fig. 8f.

Electrode	R$_s$	R$_{ct}$	W$_o$
NiFe-LDH@NF	1. 1440	0. 11079	0. 43927
NiFe-S@NF	0. 5361	0. 10668	0. 42315
CoS$_x$ @NF	0. 52701	1. 9880	0. 38407
CoS$_x$@NiFe-S@NF	0. 6235	0. 37009	0. 39492

Table S3. The numerical values of each component in the equivalent circuit of the impedance spectrum in Fig. 9g.

Electrode	R$_s$	R$_{ct}$	W$_o$
Before Cycling	1. 003	2. 013	0. 42720
After Cycling	1. 021	3. 765	0. 40556

Reference

1. J. Liao, A. Ju, W. Jiang, Y. Ju, X. Liu, N. Hu, R. Xu and J. Wang, *Electrochimica Acta*, 2022, **403**, 139605.

2. D. Xiong, M. Gu, C. Chen, C. Lu, F.-Y. Yi and X. Ma, *Chemical Engineering Journal*, 2021, **404**, 127111.

3. Y. Shao, M. F. El-Kady, J. Sun, Y. Li, Q. Zhang, M. Zhu, H. Wang, B. Dunn and R. B. Kaner, *Chemical Reviews*, 2018, **118**, 9233-9280.

4. Z.-F. Huang, J. Song, K. Li, M. Tahir, Y.-T. Wang, L. Pan, L. Wang, X. Zhang and J.-J. Zou, *Journal of the American Chemical Society*, 2016, **138**, 1359-1365.

5. X. Y. Li, K. K. Li, S. C. Zhu, K. Fan, L. L. Lyu, H. M. Yao, Y. Y. Li, J. L. Hu, H. T. Huang, Y. W. Mai and J. B. Goodenough, *Angewandte Chemie-International Edition*, 2019, **58**, 6239-6243.